# Tunable Two-Dimensional Binary Molecular Networks

*Yu Li Huang, Wei Chen,* Hui Li, Jing Ma, Jens Pflaum, and Andrew Thye Shen Wee**

***A** novel approach to constructing tunable and robust 2D binary molecular nanostructures on an inert graphite surface is presented. The guest molecules are embedded into a host molecular matrix and constrained via the formation of multiple intermolecular hydrogen bonds. By varying the binary molecular ratio and the molecular geometry, various molecular arrays with tunable intermolecular distances are fabricated. The results suggest a promising route for the fabrication of ordered and stable molecular nanostructure arrays for molecular sensors, molecular spintronic devices, and molecular p–n nanojunctions.*

**Keywords:**
- binary networks
- hydrogen bonding
- scanning tunneling microscopy
- self-assembly

## 1. Introduction

The construction of molecular nanodevices requires the precise addressing and operation of individual functioning molecules in an ordered molecular array. Molecular self-assembly on surfaces or surface-supported nanotemplates via selective and directional covalent or non-covalent interactions offers a promising bottom-up approach to fabricating molecular nanostructure arrays with desired functionalities over macroscopic areas.[1–3] Selective coupling of functional molecules to preferential adsorption sites on supporting surfaces facilitates the creation of long-range-ordered two-dimensional (2D) molecular arrays.[1–11] The directionality of selective intermolecular hydrogen bonding,[12–18] metal–ligand interactions[19–21] as well as covalent bonding[22–25] can steer the formation of ordered supramolecular assemblies with good structural stability, enabling the design and construction of a wide range of 2D molecular nanostructures such as molecular supergratings[12,13] and porous networks.[6–8,18–21,26–31] To increase the functionality and tunability of molecular nanostructure arrays, intensive efforts have been devoted to the construction of multicomponent 2D assemblies via directional intermolecular interactions.[32–38] The ultimate goal is to design robust and tunable multicomponent nanostructures whose 2D arrangements (size and overall pattern) can be controlled by experimental parameters such as the molecular geometry (size and shape) and relative molecular ratio.

The adsorption of π-conjugated organic molecules on single-crystalline metal substrates are usually stabilized through the strong interfacial coupling between the metal surface electrons and molecular π-orbitals, which can lock the adsorbed molecules at specific sites due to the corrugation of the potential energy surface of the metal substrates.[2,39–41] This restricts the lateral degrees of freedom of the adsorbed molecules and hence largely reduces the structural tunability of molecular nanostructures on metal surfaces. Inert graphite has a smooth potential-energy surface as well as relatively weak interfacial interactions with adsorbed molecules, and is therefore chosen as a supporting substrate, on which π-conjugated organic molecules have less tendency to bind to specific adsorption sites, and thereby have greater lateral degrees of freedom to assemble at their formation energy minima.[42,43] Here, we present an efficient bottom-up approach to the design and construction of tunable 2D binary molecular networks on highly oriented pyrolytic graphite (HOPG), demonstrated with binary combinations of molecules with different geometries, namely, copper hexadecafluorophthalocyanine ($F_{16}$CuPc) with *p*-sexiphenyl (6P), pentacene, or di-indenoperylene (DIP), whose molecular structures are shown in Figure 1a. These π-conjugated planar organic molecules are potential candidates

[*] Y. L. Huang, Prof. W. Chen, Dr. H. Li, Prof. A. T. S. Wee
Department of Physics
National University of Singapore
2 Science Drive 3, 117542 (Singapore)
E-mail: phycw@nus.edu.sg; phyweets@nus.edu.sg
Prof. W. Chen
Department of Chemistry
National University of Singapore
3 Science Drive 3, 117543 (Singapore)
Prof. J. Ma
Key Laboratory of Mesoscopic Chemistry of MOE
Nanjing University
Hankou Road 22, Nanjing 210093 (P.R. China)
Prof. J. Pflaum
Institute of Experimental Physics VI
University of Wuerzburg
Bavarian Center for Applied Energy Research
Am Hubland, 97047 Wuerzburg (Germany)

DOI: 10.1002/smll.200901291

NANO MICRO small

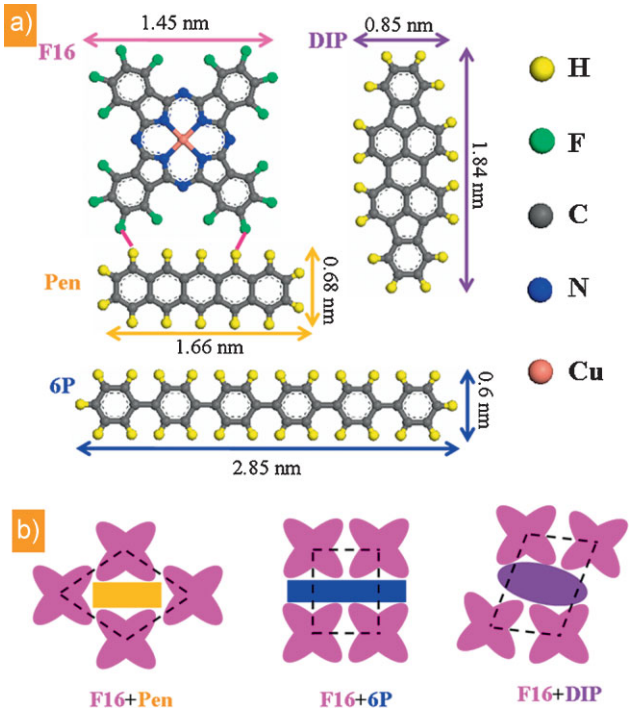


**Figure 1.** a) Molecular structures of $F_{16}$CuPc (F16), pentacene (Pen), 6P, and DIP. The short pink lines between $F_{16}$CuPc and pentacene represent the possible C–F···H–C intermolecular hydrogen bonds. b) The proposed arrangements of $F_{16}$CuPc dot arrays with pentacene (F16 + Pen), 6P (F16 + 6P), and DIP (F16 + DIP). The intermolecular separations indicated by the dashed lines are tunable by varying geometrical parameters of embedded molecules.

## 2. Results and Discussion

The first binary system presented is $F_{16}$CuPc embedded in 6P molecular matrix. As shown in the high-resolution STM images in Figure 2a–c, the long rodlike feature represents a single 6P molecule and the four-lobe feature represents an $F_{16}$CuPc molecule. Both $F_{16}$CuPc and 6P molecules lie flat on HOPG with their conjugated π-plane oriented parallel to the HOPG surface due to interfacial π–π interactions, consistent with previous reports.[44,45] Figure 2a shows the molecularly resolved STM image ($15 \times 15\ nm^2$) of the binary molecular packing structure with 6P:$F_{16}$CuPc ratio of 1:2. Two $F_{16}$CuPc doublets are interlinked by a single 6P molecule, forming oblique $F_{16}$CuPc molecular dot arrays with well-defined intermolecular distances represented by an approximately rectangular cell with $a_1 = 1.55 \pm 0.05$ nm, $b_1 = 2.27 \pm 0.05$ nm, and $\alpha_1 = 92.0 \pm 2^\circ$. The supramolecular packing structure of this $F_{16}$CuPc dot array is consistent with the expected tessellation for the 6P:$F_{16}$CuPc binary system (denoted as **F16 + 6P** in Figure 1b). The smooth surface potential of HOPG ensures that the 2D network can tolerate small lateral and rotational molecular motion to reach the formation energy minima during self-assembly. The intermolecular distance of the $F_{16}$CuPc dot array can be manipulated by controlling the 6P:$F_{16}$CuPc molecular ratio. At a higher 6P:$F_{16}$CuPc molecular ratio of 1:1, a 6P doublet bridges two $F_{16}$CuPc doublets, thereby forming an $F_{16}$CuPc array with larger oblique cell with $a_2 = 1.60 \pm 0.05$ nm, $b_2 = 2.99 \pm 0.05$ nm, and $\alpha_2 = 96.0 \pm 4^\circ$, as shown in Figure 2b. By further increasing the 6P:$F_{16}$CuPc molecular ratio to 3:1 (Figure 2c), the enlarged oblique $F_{16}$CuPc

in bulk heterojunction photovoltaic cells or as controlled injection barriers in organic thin-film devices.[10,43] In this report, these prototype molecular systems are used to study the tunability of 2D molecular arrangements with varying geometrical parameters. As illustrated in Figure 1b, the intermolecular separations of $F_{16}$CuPc dot arrays are tunable by embedding different molecular spacers. Using in situ low-temperature scanning tunneling microscopy (LT-STM) imaging, we demonstrate that the binary molecular networks can be effectively tuned by varying the molecular geometrical parameters as well as the relative molecular ratios. Theoretical simulations based on density functional theory (DFT) are employed to evaluate the intermolecular binding energies and to rationalize the stability of these networks. We show that the formation of multiple intermolecular C–F···H–C hydrogen bonds between the electronegative periphery F atoms of $F_{16}$CuPc and the electropositive periphery H atoms of 6P, pentacene, or DIP, enhances the structural stability of these tunable $F_{16}$CuPc molecular dot arrays.

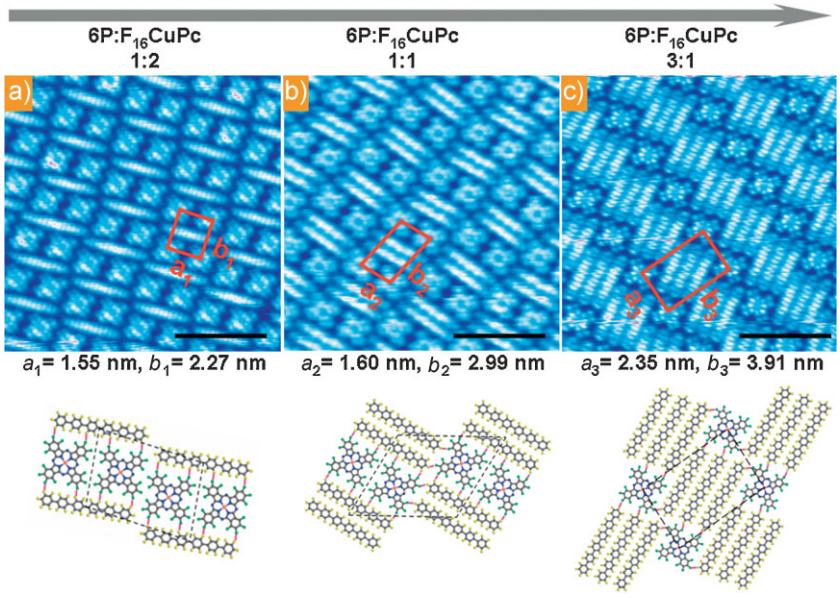


**Figure 2.** Top) Molecularly resolved $15 \times 15\text{-nm}^2$ STM images of the oblique $F_{16}$CuPc molecular dot arrays with tunable intermolecular distance controlled by the 6P coverage. The oblique $F_{16}$CuPc molecular dot arrays comprise two $F_{16}$CuPc doublets interlinked by a) a 6P monomer molecule at low 6P coverage of 6P:$F_{16}$CuPc = 1:2 ($V_{tip} = 2.0$ V), b) a 6P doublet by increasing the molecular ratio of 6P:$F_{16}$CuPc to 1:1 ($V_{tip} = 2.0$ V), and c) a 6P triplet at the high 6P coverage of 6P:$F_{16}$CuPc = 3:1 ($V_{tip} = 2.7$ V). The scale bar in each STM image represents 5 nm. Bottom) The simulated molecular packing structures of the different oblique $F_{16}$CuPc molecular dot arrays. The short pink lines between $F_{16}$CuPc and 6P represent the possible C–F···H–C intermolecular hydrogen bonds. The blue dashed parallelograms indicate the primitive unit cells.

molecular dot array forms two $F_{16}CuPc$ doublets interconnected by a 6P triplet forming an approximately rectangular cell with $a_3 = 2.35 \pm 0.05$ nm, $b_3 = 3.91 \pm 0.05$ nm, and $\alpha_3 = 91.0 \pm 2^\circ$. This series of experiments clearly demonstrates the geometrical tunability of the $F_{16}CuPc$ molecular dot arrays by controlling the 6P:$F_{16}CuPc$ molecular ratios. The corresponding simulated molecular superstructures are given below each STM image in Figure 2 (simulation details are discussed below). The possible intermolecular C–F...H–C hydrogen bonds with F...H distances of ≈2.5–2.6 Å are highlighted by the pink lines, the bond lengths of which are typical of weak hydrogen bonds.[46]

The second system is shown in Figure 3, whereby the intermolecular separation of the $F_{16}CuPc$ molecular dot array is manipulated by intermixing $F_{16}CuPc$ with pentacene (Pen), whose molecular length is almost half the length of 6P (Figure 1). Figure 3 shows selected molecularly resolved $10 \times 10$-nm$^2$ STM images of the supramolecular packing structures at different Pen:$F_{16}CuPc$ ratios. The bright short rodlike feature represents a single pentacene molecule. The oblique cell of $c_1 = 1.84 \pm 0.05$ nm, $d_1 = 1.86 \pm 0.05$ nm, and $\beta_1 = 79.0 \pm 2^\circ$ at a Pen:$F_{16}CuPc$ ratio of 1:1 (Figure 3a) can be enlarged to $c_2 = 2.24 \pm 0.05$ nm, $d_2 = 2.15 \pm 0.05$ nm, and $\beta_2 = 81.0 \pm 2^\circ$ at a Pen:$F_{16}CuPc$ ratio of 2:1 (Figure 3b), and further enlarged to $c_3 = 2.89 \pm 0.05$ nm, $d_3 = 2.88 \pm 0.05$ nm, and $\beta_3 = 72.0 \pm 2^\circ$ at a higher Pen:$F_{16}CuPc$ ratio of 4:1 (Figure 3c). From Figure 3c, we note that the dimensions of the pentacene doublet are comparable to that of the square $F_{16}CuPc$ molecule. The in-plane orientation of the pentacene doublet can spontaneously switch between two different orientations in the Pen:$F_{16}CuPc$ networks at ratios of 4:1 and above, and therefore lack long-range order (images not shown). This suggests that the geometrical similarity between a single $F_{16}CuPc$ molecule and a pentacene doublet increases the rotational freedom of the pentacene doublet in binary molecular networks.

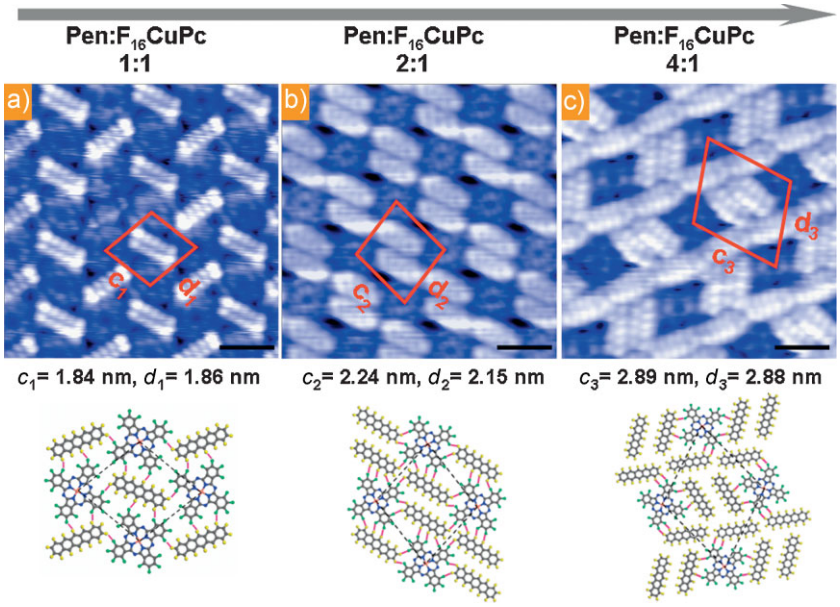


**Figure 3.** Molecularly resolved $10 \times 10$-nm$^2$ STM images of the $F_{16}CuPc$ molecular dot arrays with tunable intermolecular distance controlled by the pentacene (Pen) coverage. a) Pen:$F_{16}CuPc$ = 1:1 ($V_{tip}$ = 2.5 V); b) Pen:$F_{16}CuPc$ = 4:1 ($V_{tip}$ = 3.0 V); c) Pen:$F_{16}CuPc$ = 4:1 ($V_{tip}$ = 2.8 V). The short rodlike bright feature represents pentacene molecule. The scale bar in each STM image represents 2 nm. The DFT simulated molecular models are shown below each STM image.

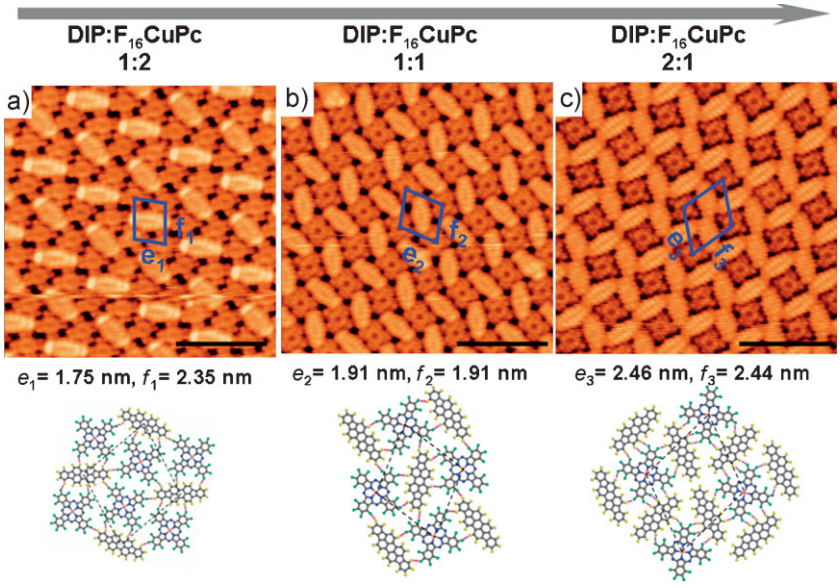


**Figure 4.** Molecularly resolved $15 \times 15$-nm$^2$ STM images (top) and DFT simulated molecular models (below) of the $F_{16}CuPc$ molecular dot arrays with tunable intermolecular distance controlled by the DIP coverage. a) DIP:$F_{16}CuPc$ = 1:2 ($V_{tip}$ = 2.8 V); b) DIP:$F_{16}CuPc$ = 1:1 ($V_{tip}$ = 2.0 V); c) DIP:$F_{16}CuPc$ = 2:1 ($V_{tip}$ = 2.0 V). The leaflike bright feature represents a DIP molecule. The scale bar in each STM image represents 5 nm.

The tunability of self-assembled molecular nanostructures on HOPG is further demonstrated by the third binary system of $F_{16}CuPc$ with DIP. Since DIP is an elliptical molecule with different dimensions to 6P and pentacene (Figure 1), the intermixing of $F_{16}CuPc$ with DIP results in $F_{16}CuPc$ dot arrays with different intermolecular separations and arrangements. As shown in Figure 4, the bright leaflike feature represents a single DIP molecule. The structure of this binary supramolecular network, or the intermolecular distance of the $F_{16}CuPc$ dot arrays, can be effectively adjusted by controlling the DIP:$F_{16}CuPc$ ratio. The unit cell dimensions vary from $e_1 = 1.75 \pm 0.05$ nm, $f_1 = 2.35 \pm 0.05$ nm, and $\gamma_1 = 82.0 \pm 2^\circ$ at the DIP:$F_{16}CuPc$ ratio of 1:2 (Figure 4a), $e_2 = 1.91 \pm 0.05$ nm, $f_2 = 1.91 \pm 0.05$ nm, and $\gamma_2 = 77.0 \pm 2^\circ$ at

NANO MICRO small

**Table 1.** Energy profile of the binary molecular networks on HOPG surface. $E_{A-B}$ presents the intermolecular binding energy of the neighboring *A* and *B* molecules, where *A* and *B* represent $F_{16}$CuPc, Pen, 6P, or DIP molecules, independently. $E_{bind}$ is the total intermolecular binding energy of each primitive cell as indicated in the simulated supramolecular packing structures. All energies are given in [kcal mol$^{-1}$].

| 6P:$F_{16}$ | $E_{F16-F16}$ | $E_{6P-6P}$ | $E_{F16-6P}$ | $E_{bind}$ | No. of H-bonds(<2.6 Å) |
|---|---|---|---|---|---|
| 1:2 | −0.73 | – | −14.78 | −15.51 | 8 |
| 1:1 | −1.17 | 2.10 | −18.70 | −17.77 | 12 |
| 3:1 | – | 6.29 | −13.84 | −7.55 | 6 |
| Pen:$F_{16}$ | $E_{F16-F16}$ | $E_{Pen-Pen}$ | $E_{F16-Pen}$ | $E_{bind}$ | No. of H-bonds(<2.6 Å) |
| 1:1 | – | – | −12.12 | −12.12 | 6 |
| 2:1 | – | 0.65 | −19.48 | −18.83 | 12 |
| 4:1 | – | 2.97 | −13.92 | −10.95 | 8 |
| DIP:$F_{16}$ | $E_{F16-F16}$ | $E_{DIP-DIP}$ | $E_{F16-DIP}$ | $E_{bind}$ | No. of H-bonds(<2.6 Å) |
| 1:2 | 0.25 | – | −13.74 | −13.49 | 8 |
| 1:1 | – | – | −13.86 | −13.86 | 6 |
| 2:1 | – | 0.64 | −19.26 | −18.62 | 10 |

the ratio of 1:1 (Figure 4b), and $e_3 = 2.46 \pm 0.05$ nm, $f_3 = 2.44 \pm 0.05$ nm, and $\gamma_3 = 72.0 \pm 2^\circ$ at the ratio of 2:1 (Figure 4c). In Figure 4c, each $F_{16}$CuPc molecule is surrounded by four DIP molecules, which maximizes the number of the C–F...H–C intermolecular hydrogen bonds, giving good structural stability of this binary molecular network. Our simulated molecular models, shown below each STM image, suggest that the DIP:$F_{16}$CuPc binary molecular system has the number of possible hydrogen bonds of ten in the primitive unit cell when the intermixing ratio reaches 2:1 (listed in Table 1). Similar DIP and $F_{16}$CuPc binary networks combined though multiple intermolecular C–F...H–C bonding have also been reported on Au(111) and Cu(111) surfaces.[47]

To better understand the structural stability of these binary systems, DFT calculations were performed to evaluate the total intermolecular binding energy ($E_{bind}$) of each observed network. It is found that the molecule/graphite interfaces are dominated by π–π interactions, which constrain the molecules to lie flat with their conjugated π-plane parallel to the surface. The smooth potential-energy surface of graphite does not induce any interlocking of adsorbed molecules with the substrate lattice. The 2D arrangements of the molecular networks are therefore mainly determined by the lateral intermolecular interactions. We first construct supramolecular packing structures on HOPG slabs based on the optimized intermolecular F...H (≈2.5 Å) and F...F (≈2.7 Å) distances[48] as well as the structural symmetry observed in the STM images. The constructed molecular models agree well with our experimental results with deviations of less than 5%, as shown in Figures 2, 3, and 4. All the calculations are on B3LYP[49,50]/6-31G(d,p) level with the Gaussian03 package.[51] In Table 1, we divide the formation energy $E_{bind}$ into three parts, binding energies originating from $F_{16}$CuPc–$F_{16}$CuPc ($E_{F16-F16}$), *X*–*X* ($E_{X-X}$), and $F_{16}$CuPc–*X* ($E_{F16-X}$) intermolecular interactions (*X* represents 6P, pentacene, or DIP). It is obvious that the $E_{bind}$ for each network is dominated by the $F_{16}$CuPc–*X* interactions ($E_{F16-X}$), confirming that the stability of these $F_{16}$CuPc dot arrays is greatly enhanced by intermolecular C–F...H–C bonding. In each primitive unit cell, the number of possible C–F...H–C intermolecular hydrogen bonds with a maximum length of 2.6 Å is also given in Table 1. Hence, the DFT calculations support our hypothesis that the formation of multiple intermolecular hydrogen bonds stabilizes these binary molecular networks.

## 3. Conclusions

We have demonstrated a novel bottom-up approach to fabricate self-assembled 2D binary molecular networks on graphite, whose structural stability is sustained through the formation of multiple intermolecular C–F...H–C hydrogen bonds between the electronegative periphery F atoms of $F_{16}$CuPc and the electropositive periphery H atoms of 6P, pentacene, or DIP. The supramolecular packing structures can be controlled by careful selection of molecular building blocks with appropriate geometry (size and shape) and molecular ratios. Our DFT calculations confirm that the intermolecular hydrogen bonding drives the formation of these molecular nanostructure arrays towards their energy-minima configurations. Using this approach, we demonstrate the fabrication of ordered and robust molecular nanostructure arrays with a high degree of tunability. Such molecular nanostructures have potential applications in molecular sensors and nanodevices. In particular, the versatility of the metal phthalocyanines allows the ease of modification of the central metal atoms to feature desired functionalities, such as electronic spins for the construction of molecular spintronic devices.

## 4. Experimental Section

The LT-STM experiment was carried out in an Omicron LT-STM interfaced to a Nanonis controller. [8–10, 47] All STM imaging was performed at 77 K. Freshly cleaved HOPG substrate was thoroughly degassed in UHV at around 800 K overnight before deposition. 6P, DIP, pentacene, and $F_{16}$CuPc were sequentially deposited from low-temperature Knudsen cells onto HOPG at room temperature (RT) in a separated growth chamber. Prior to the deposition, 6P, DIP, pentacene, and $F_{16}$CuPc were purified twice by gradient vacuum sublimation. The deposition rates of 6P, DIP, and pentacene (0.01 ML min$^{-1}$) and $F_{16}$CuPc (0.03 ML min$^{-1}$) were monitored by a quartz crystal microbalance (QCM) during evaporation, and were further calibrated by counting the

  

adsorbed-molecule coverage in large-scale LT-STM images at coverages below 1 monolayer (1 ML = one full monolayer of close packed 6P, DIP, pentacene, or $F_{16}$CuPc with their conjugated $\pi$-plane oriented parallel to the HOPG surface).

## Acknowledgements

*The authors acknowledge support from the Singapore A*STAR grant of R-398-000-036-305, ARF grants R-144-000-196-112, R-143-000-392-133 and R-143-000-406-112. This work was also supported by National Natural Science Foundation of China (No. 20825312) and Fok Ying Tong Education Foundation (No. 111013).*

[1] J. V. Barth, G. Constantini, K. Kern, *Nature* **2005**, *437*, 671–679.
[2] J. V. Barth, *Annu. Rev. Phys. Chem.* **2007**, *58*, 375–407.
[3] a) S.-S. Li, B. H. Northrop, Q. H. Yuan, L. J. Wan, P. J. Stang, *Acc. Chem. Res.* **2009**, *42*, 249–259; b) L. J. Wan, *Acc. Chem. Res.* **2006**, *39*, 334–342.
[4] F. Cicoira, C. Santato, F. Rosei, *Topics Curr. Chem.* **2008**, *285*, 203–267.
[5] F. Rosei, *J. Phys. Condens. Matt.* **2004**, *16*, S1373–S1436.
[6] J. A. Theobald, N. S. Oxtoby, M. A. Phillips, N. R. Champness, P. H. Beton, *Nature* **2003**, *424*, 1029–1031.
[7] S. Stepanow, N. Lin, J. V. Barth, K. Kern, *Chem. Commun.* **2006**, 2153–2155.
[8] H. L. Zhang, W. Chen, H. Huang, L. Chen, A. T. S. Wee, *J. Am. Chem. Soc.* **2008**, *130*, 2720–2721.
[9] H. L. Zhang, W. Chen, L. Chen, H. Huang, J. Yuhara, A. T. S. Wee, *Small* **2007**, *3*, 2015–2018.
[10] W. Chen, H. L. Zhang, H. Huang, L. Chen, A. T. S. Wee, *Appl. Phys. Lett.* **2008**, *92*, 193301.
[11] M. Corso, W. Auwärter, M. Muntwiler, A. Tamai, T. Greber, J. Osterwalder, *Science* **2004**, *303*, 217–220.
[12] J. Weckesser, A. De Vita, J. V. Barth, C. Cai, K. Kern, *Phys. Rev. Lett.* **2001**, *87*, 096101.
[13] J. V. Barth, J. Weckesser, C. Z. Cai, P. Günter, L. Bürgi, O. Jeandupeux, K. Kern, *Angew. Chem, Int. Ed.* **2000**, *39*, 1230–1234.
[14] a) R. Otero, M. Schöck, L. M. Molina, E. Lægsgaard, I. Stensgaard, B. Hammer, F. Besenbacher, *Angew. Chem. Int. Ed.* **2004**, *44*, 2270–2275; b) R. Otero, M. Lukas, R. E. A. Kelly, W. Xu, E. Lægsgaard, I. Stensgaard, L. N. Kantorovich, F. Besenbacher, *Science* **2008**, *319*, 312–315.
[15] A. Llanes-Pallas, M. Matena, T. Jung, M. Prato, M. Stohr, D. Bonifazi, *Angew. Chem. Int. Ed.* **2008**, *47*, 7726–7731.
[16] T. Yokoyama, S. Yokoyama, T. Kamikado, Y. Okuno, S. Mashiko, *Nature* **2001**, *413*, 619–621.
[17] L. M. A. Perdigao, N. R. Champness, P. H. Beton, *Chem. Commun* **2006**, 538–540.
[18] M. Stohr, M. Wahl, H. Spillmann, L. H. Gade, T. A. Jung, *Small* **2007**, *3*, 1336–1340.
[19] a) S. Stepanow, M. A. Lingenfelder, A. Dmitriev, H. Spillmann, E. Delvigne, N. Lin, X. Deng, C. Cai, J. V. Barth, K. Kern, *Nat. Mater.* **2004**, *3*, 229–233; b) M. A. Lingenfelder, H. Spillmann, A. Dmitriev, S. Stepanow, N. Lin, J. V. Barth, K. Kern, *Chem. Eur. J.* **2004**, *10*, 1913–1919.
[20] a) N. Lin, S. Stepanow, F. Vidal, J. V. Barth, K. Kern, *Chem. Commun.* **2005**, 1681–1683; b) N. Lin, A. Langner, S. L. Tait, R. Chandrasekar, M. Ruben, K. Kern, *Chem. Commun.* **2007**, 4860–4862; c) A. Langner, S. L. Tait, N. Lin, R. Chandrasekar, M. Ruben, K. Kern, *Angew. Chem. Int. Ed.* **2008**, *47*, 8835–8838; d) A. Langner, S. L. Tait, N. Lin, R. Chandrasekar, M. Ruben, K. Kern, *Proc. Natl. Acad. Sci. USA* **2007**, *104*, 17927–17930.
[21] U. Schlickum, R. Decker, F. Klappenberger, G. Zoppellaro, S. Klyatskaya, M. Ruben, I. Silanes, A. Arnau, K. Kern, H. Brune, J. V. Barth, *Nano Lett.* **2007**, *7*, 3813–3817.
[22] D. F. Perepichka, F. Rosei, *Science* **2009**, *323*, 216–217.
[23] L. Grill, M. Dyer, L. Lafferentz, M. Persson, M. V. Peters, S. Hecht, *Nat. Nanotechnol.* **2007**, *2*, 687–691.
[24] M. Treier, N. V. Richardson, R. Fasel, *J. Am. Chem. Soc.* **2008**, *130*, 14054–14055.
[25] A. Gourdon, *Angew. Chem. Int. Ed.* **2008**, *47*, 6950–6953.
[26] R. Madueno, M. T. Raisanen, C. Silien, M. Buck, *Nature* **2008**, *454*, 618–621.
[27] a) J. C. Swarbrick, B. L. Rogers, N. R. Champness, P. H. Beton, *J. Phys. Chem. B* **2006**, *110*, 6110–6114; b) J. Ma, B. L. Rogers, M. J. Humphry, D. J. Ring, G. Goretzki, N. R. Champness, P. H. Beton, *J. Phys. Chem. B* **2006**, *110*, 12207–12210; c) P. A. Staniec, L. M. A. Perdigao, A. Saywell, N. R. Champness, P. H. Beton, *ChemPhysChem* **2007**, *8*, 2177–2181; d) P. A. Staniec, L. M. A. Perdigao, B. L. Rogers, N. R. Champness, P. H. Beton, *J. Phys. Chem. C* **2007**, *111*, 886–893.
[28] S. B. Lei, K. Tahara, X. L. Feng, S. Furukawa, F. C. De Schryver, K. Müllen, Y. Tobe, S. De Feyter, *J. Am. Chem. Soc.* **2008**, *130*, 7119–7129.
[29] G. Pawin, K. L. Wong, K. Y. Kwon, L. Bartels, *Science* **2006**, *313*, 961–962.
[30] H. Spillmann, A. Kiebele, M. Stohr, T. A. Jung, D. Bonifazi, F. Cheng, F. Diederich, *Adv. Mater.* **2006**, *18*, 275–279.
[31] W. D. Xiao, X. L. Feng, P. Ruffieux, O. Groning, K. Müllen, R. Fasel, *J. Am. Chem. Soc.* **2008**, *130*, 8910–8912.
[32] W. Chen, H. Li, H. Huang, Y. X. Fu, H. L. Zhang, J. Ma, A. T. S. Wee, *J. Am. Chem. Soc.* **2008**, *130*, 12285–12289.
[33] L. Kampschulte, T. L. Werblowsky, R. S. K. Kishore, M. Schmittel, W. M. Heckl, M. Lackinger, *J. Am. Chem. Soc.* **2008**, *130*, 8502–8507.
[34] S. B. Lei, M. Surin, K. Tahara, J. Adisoejoso, R. Lazzaroni, Y. Tobe, S. De Feyter, *Nano Lett.* **2008**, *8*, 2541–2546.
[35] M. E. Canas-Ventura, W. D. Xiao, D. Wasserfallen, K. Müllen, H. Brune, J. V. Barth, R. Fasel, *Angew. Chem. Int. Ed.* **2007**, *46*, 1814–1818.
[36] F. Silly, A. Q. Shaw, M. R. Castell, G. A. D. Briggs, *Chem. Commun.* **2008**, *1907*, 1909.
[37] a) K. W. Hipps, L. Scudiero, D. E. Barlow, M. P. Cooke, Jr, *J. Am. Chem. Soc.* **2002**, *124*, 2126–2127; b) L. Scudiero, K. W. Hipps, D. E. Barlow, *J. Phys. Chem. B* **2003**, *107*, 2903–2909.
[38] a) K. Suto, S. Yoshimoto, K. Itaya, *J. Am. Chem. Soc.* **2003**, *125*, 14976–14977; b) S. Yoshimoto, A. Tada, K. Suto, S.-L. Yau, K. Itaya, *Langmuir* **2004**, *20*, 3159–3165; c) K. Suto, S. Yoshimoto, K. Itaya, *Langmuir* **2006**, *22*, 10766–10776; d) S. Yoshimoto, Y. Honda, O. Ito, K. Itaya, *J. Am. Chem. Soc.* **2008**, *130*, 1085–1092.
[39] U. K. Weber, V. M. Burlakov, L. M. A. Perdigao, R. H. J. Fawcett, P. H. Beton, N. R. Champness, J. H. Jefferson, G. A. D. Briggs, D. G. Pettifor, *Phys. Rev. Lett.* **2008**, *100*, 156101.
[40] V. Oison, M. Koudia, M. Abel, L. Porte, *Phys. Rev. B* **2007**, *75*, 035428.
[41] S. Lukas, G. Witte, Ch, Wöll, *Phys. Rev. Lett.* **2002**, *88*, 028301.
[42] F. Ortmann, W. G. Schmidt, F. Bechstedt, *Phys. Rev. Lett.* **2005**, *95*, 186101.
[43] D. G. de Oteyza, T. N. Krauss, E. Barrena, S. Sellner, H. Dosch, J. O. Osso, *Appl. Phy. Lett.* **2007**. *90*, 243104.
[44] W. Chen, H. Huang, A. T. S. Wee, *Chem. Commun.* **2008**, 4276–4278.

  

[45] Y. L. Huang, W. Chen, S. Chen, A. T. S. Wee, *Appl. Phys. A* **2009**, *95*, 107–111.
[46] T. S. Steiner, *Angew. Chem. Int. Ed.* **2002**, *41*, 48–76.
[47] E. Barrena, D. G. de Oteyza, H. Dosch, Y. Wakayama, *ChemPhysChem* **2007**, *8*, 1915–1918.
[48] The intermolecular F...F and F...H distances are obtained from optimized structures of $C_6F_6$–$C_6F_6$ (fluorinated benzene) pair and $C_6F_6$–$C_6H_6$ (benzene) molecular pair absorbed on HOPG slabs, respectively.
[49] A. D. Becke, *J. Chem. Phys.* **1993**, *98*, 5648–5652.
[50] C. Lee, W. Yang, R. G. Parr, *Phys. Rev. B* **1988**, *37*, 785–789.
[51] M. J. Frisch, G. W. Trucks, H. B. Schlegel, G. E. Scuseria, M. A. Robb, J. R. Cheeseman, J. A. Montgomery, Jr., T. Vreven, K. N. Kudin, J. C. Burant, J. M. Millam, S. S. Iyengar, J. Tomasi, V. Barone, B. Mennucci, M. Cossi, G. Scalmani, N. Rega, G. A. Petersson, H. Nakatsuji, M. Hada, M. Ehara, K. Toyota, R. Fukuda, J. Hasegawa, M. Ishida, T. Nakajima, Y. Honda, O. Kitao, H. Nakai, M. Klene, X. Li, J. E. Knox, H. P. Hratchian, J. B. Cross, V. Bakken, C. Adamo, J. Jaramillo, R. Gomperts, R. E. Stratmann, O. Yazyev, A. J. Austin, R. Cammi, C. Pomelli, J. W. Ochterski, P. Y. Ayala, K. Morokuma, G. A. Voth, P. Salvador, J. J. Dannenberg, V. G. Zakrzewski, S. Dapprich, A. D. Daniels, M. C. Strain, O. Farkas, D. K. Malick, A. D. Rabuck, K. Raghavachari, J. B. Foresman, J. V. Ortiz, Q. Cui, A. G. Baboul, S. Clifford, J. Cioslowski, B. B. Stefanov, G. Liu, A. Liashenko, P. Piskorz, I. Komaromi, R. L. Martin, D. J. Fox, T. Keith, M. A. Al-Laham, C. Y. Peng, A. Nanayakkara, M. Challacombe, P. M. W. Gill, B. Johnson, W. Chen, M. W. Wong, C. Gonzalez, J. A. Pople, Gaussian 03, D.01; Gaussian, Inc: Wallingford, CT 2004.

Received: July 21, 2009
Revised: September 16, 2009
Published online: November 9, 2009